

SMP-RCR: A Sparse Multipoint Moment Matching Method for RC Reduction

Siyuan Yin, Yuncheng Xu, Lin Liu, Fan Yang, *Member, IEEE*, Xuan Zeng, *Senior Member, IEEE*, Chengtao An^{*} and Yangfeng Su^{*}

Abstract—In post-layout circuit simulation, efficient model order reduction (MOR) for many-port resistor-capacitor (RC) circuits remains a crucial issue. The current mainstream MOR methods for such circuits include high-order moment matching methods and elimination methods. High-order moment matching methods—characterized by high accuracy, such as PRIMA and TurboMOR—tend to generate large dense reduced-order systems when the number of ports is large, which impairs the efficiency of MOR. Another common type of MOR method for many-port circuits is based on Gaussian elimination, with the SIP method as a representative. The main limitation of this method lies in the inadequate matching of high-order moments. In this paper, we propose a sparse multipoint moment matching method and present comprehensive theoretical analysis results regarding the multi-frequency high-order moment matching property. Meanwhile, to enhance the algorithm’s efficiency, sparse control and deflation techniques are introduced to further optimize the algorithm. Numerical experiments demonstrated that, compared to SIP, the accuracy is improved by more than two orders of magnitude at high frequency points without adding many extra linear components. Compared to TurboMOR methods, our method achieves a speed improvement of more than twice while maintaining the same level of precision.

Index Terms—Model Order Reduction, Multipoint Moment Matching, Sparsification, Multi-port RC Reduction

I. INTRODUCTION

In post-layout circuit simulation, a large number of parasitic resistors and capacitors are extracted after parameter extraction, which means we need to solve extremely large-scale nonlinear systems. This process is highly time-consuming. Model order reduction methods for nonlinear systems, as listed in [1], [2], are used to construct approximate reduced nonlinear systems to speed up post-layout circuit simulation. However, methods such as proper orthogonal decomposition (**POD**) [3]–[5] or balanced truncation (**TBR**) [6]–[8] are both computationally expensive when constructing the reduced model. To address this issue, nonlinear nodes are preserved, and the extracted parasitic resistor-capacitor (**RC**) networks are reduced using RC reduction (**RCR**) techniques [9] while ensuring the accuracy remains acceptable.

A kind of **RCR** method with high accuracy is based on **Krylov** subspace. This kind of method constructs an orthog-

onal basis by **Arnoldi** procedure or **Lanczos** procedure and obtains the reduced system by projecting the original state space onto this subspace spanned by the orthogonal basis. **PRIMA** [10] is based on the block **Arnoldi** procedure and **MPVL** [11] is based on **Lanczos** procedure, they can both match multiple moments on single point. Another kind of method with high accuracy is multipoint moment matching based methods based on rational **Lanczos** procedure [12] are proposed in [13] and [14]. However, it is important to note that the reduced systems generated by these methods are dense.

Another method, called **TurboMOR-RC**, which can match multiple moments, was proposed in [15]. The reduced systems obtained by these methods have a block tridiagonal structure. The size of the reduced systems generated by the above methods grows proportionally with the number of ports, leading to a decrease in the efficiency of model order reduction as the number of ports increases.

A commonly used method for reducing the order of multi-port **RC** circuits is based on Gaussian elimination, with methods such as **SIP** [16]–[18], **PACT** [19], and **TICER** [20]–[22] as representatives. These methods yield reduced-order systems whose dimension is independent of the number of ports. However, these methods currently face the challenge of low accuracy. From a theoretical perspective, these methods possess the property of matching up to the first two moments, but this may not always be sufficient in practical simulation processes involving high frequencies.

Aggregation based methods such as **AMOR** [23] which apply spectral clustering [24] to aggregate internal nodes and **RC-in-RC-out** method [25] is also efficient for **RC** circuits with many ports. These methods generate sparse reduced systems without introducing fill-ins or negative elements. However, different from elimination based methods, these methods have no accuracy guarantee for moment match.

In this article, we 1) propose a framework to generate a reduced system with high accuracy for a many-port **RC** circuit based on elimination at multiple points; 2) present the multipoint moment matching theorem of the framework; 3) propose the implementation techniques including sparsity control and deflation to render the reduced system sparse. Numerical experiments show that, compared to **SIP**, our method delivers an accuracy improvement of more than two orders of magnitude at high-frequency points without introducing a large number of additional linear components. When benchmarked against **TurboMOR** methods, our approach reduces the number of non-zero elements by over 60% and achieves a speedup of more than double, all while maintaining the same level of

^{*} Corresponding authors: Yangfeng Su, Email: yfsu@fudan.edu.cn and Chengtao An, Email: ancht@empyrean.com.cn

¹ Siyuan Yin, Yuncheng Xu and Yangfeng Su are with School of Mathematical Sciences, Fudan University, China.

² Lin Liu and Chengtao An are with Empyrean, China.

³ Fan Yang and Xuan Zeng are with State Key Lab of Integrated Chips and Systems, College of Integrated Circuits and Micro-Nano Electronics, Fudan University, China.

accuracy and retaining the block tridiagonal structure.

The rest of this paper is organized as follows. In Section 2, we describe the **MOR** problem for many-port **RC** circuits and review the **TurboMOR** algorithm. In Section 3, we introduce our multipoint moment matching model order reduction framework and provide corresponding moment matching theorem. Section 4 introduces implementation techniques for algorithm. Section 5 presents the numerical experiments, where our method is compared with commonly used **MOR** methods. In Section 6, we draw our conclusions, and in the Appendix, we provide some mathematical proofs and details.

II. PRELIMINARIES

In this section, we mainly introduce the basic concepts of **RC** reduction and the fundamental notation. To facilitate comparison with the **TurboMOR** method, we also review the process of the **TurboMOR** algorithm for **RC** reduction.

A. RC Reduction and Moment Matching

The original system for model order reduction is derived from an **RC** circuit with n nodes, including p ports. By applying modified nodal analysis (**MNA**) [26], the original system can be represented by the following differential algebraic equations:

$$\begin{cases} C\dot{x}(t) + Gx(t) = Bu(t) \\ y(t) = B^\top x(t) \end{cases}, \quad (1)$$

where matrices $G \in \mathbb{R}^{n \times n}$, $C \in \mathbb{R}^{n \times n}$ are symmetric, nonnegative definite, representing the conductance matrix and capacitance matrix, respectively. Vector $x \in \mathbb{R}^n$ contains nodal voltages. Matrix $B \in \mathbb{R}^{n \times p}$ denotes the index of the ports and there exists a permutation matrices P, Q such that

$$PBQ = \begin{bmatrix} I_p \\ 0 \end{bmatrix}.$$

Vector $u \in \mathbb{R}^p$ and $y \in \mathbb{R}^p$ represent port currents and port voltages, respectively. Transfer function is used to describe the input-output relationship and the original transfer function is written as

$$H(s) = B^\top (G + sC)^{-1} B. \quad (2)$$

It can be verified that $H(s)$ is invariant when we permute the nodes.

MOR for original system (1) involves finding a transformation matrix $V \in \mathbb{R}^{n \times r}$ and projection matrix $W \in \mathbb{R}^{n \times r}$, and $W^\top V = I_r$ is satisfied usually. Afterwards, the reduced model is generated by the approximation $x(t) \approx V\hat{x}(t)$ and the residuals of the state equations in system (1) are orthogonal to W . To preserve the symmetry of reduced conductance matrix and reduced capacitance matrix, we set $W = V$. Therefore, the reduced system can be written as

$$\begin{cases} \hat{C}\dot{\hat{x}}(t) + \hat{G}\hat{x}(t) = \hat{B}u(t) \\ \hat{y}(t) = \hat{B}^\top \hat{x}(t) \end{cases}, \quad (3)$$

where matrices $\hat{G} = V^\top GV \in \mathbb{R}^{r \times r}$, $\hat{C} = V^\top CV \in \mathbb{R}^{r \times r}$, vector $\hat{x} \in \mathbb{R}^r$, matrix $\hat{B} \in \mathbb{R}^{r \times p}$, and $r < n$. The transfer function of system (3) is

$$\hat{H}(s) = \hat{B}^\top (\hat{G} + s\hat{C})^{-1} \hat{B}. \quad (4)$$

In order to meet the requirements of circuit simulation, a satisfactory reduced-order system typically needs to satisfy the following properties:

- Reduced system approximates original system well;
- Reduced system simulates faster than original system;
- Some properties of original systems such as passivity and symmetry are preserved;
- All the ports should be preserved, which means that matrix \hat{B} can be seen as the result of removing some zero rows from matrix B .

To measure the accuracy of the reduced-order system, we introduce the concept of the moment [27] of the transfer function. Let $A \equiv G + s_0C$ and expand the transfer function eq. (2) at $s_0 \in \mathbb{R}_+$:

$$H(s) = \sum_{k=0}^{+\infty} (-1)^k B^\top (A^{-1}C)^k A^{-1}B(s - s_0)^k,$$

the moment of the k th order at s_0 is defined as

$$M_k(s_0) \equiv (-1)^k B^\top (A^{-1}C)^k A^{-1}B.$$

Similarly, we can define the moment of the reduced transfer function (4):

$$\hat{M}_k(s_0) \equiv (-1)^k \hat{B}^\top (\hat{A}^{-1}\hat{C})^k \hat{A}^{-1}\hat{B},$$

where $\hat{A} = \hat{G} + s_0\hat{C}$. It has been proven in [16] that the reduced system generated by **SIP** matches the first 2 moments at $s_0 = 0$ of original system.

B. TurboMOR-RC

The **TurboMOR** method further improves the accuracy based on the elimination method, while ensuring that the reduced-order system has a block tridiagonal structure.

Suppose the coefficient matrix of the original system (1) has the following block partition:

$$G = \begin{bmatrix} G_p & G_C^\top \\ G_C & G_I \end{bmatrix}, C = \begin{bmatrix} C_p & C_C^\top \\ C_C & C_I \end{bmatrix}, B = \begin{bmatrix} I_p \\ 0 \end{bmatrix}.$$

The first step of the algorithm is to completely decouple all internal nodes of the system through congruence transformation. Assume the **Cholesky** factor of G_I is K , and the congruence transformation is formulated as

$$Q^{(1)} = \begin{bmatrix} I_p & \\ -K^{-\top} K^{-1} G_C & K^{-\top} \end{bmatrix}.$$

Then we have

$$G^{(1)} \equiv Q^{(1)\top} G Q^{(1)} = \begin{bmatrix} G_p^{(1)} & \\ & I_{n-p} \end{bmatrix};$$

$$\begin{bmatrix} G_p^{(1)} & & \\ & I_p & \\ & & \ddots & \\ & & & I_p \end{bmatrix} \begin{bmatrix} x_p^{(1)}(s) \\ x_p^{(2)}(s) \\ \vdots \\ x_p^{(r)}(s) \end{bmatrix} + s \begin{bmatrix} C_p^{(1)} & R^{(2)\top} & \\ R^{(2)} & C_p^{(2)} & \ddots \\ & \ddots & R^{(r)\top} \\ & & C_p^{(r)} \end{bmatrix} \begin{bmatrix} x_p^{(1)}(s) \\ x_p^{(2)}(s) \\ \vdots \\ x_p^{(r)}(s) \end{bmatrix} = \begin{bmatrix} B \\ 0 \\ \vdots \\ 0 \end{bmatrix} u(s) \quad (5)$$

$$C^{(1)} \equiv Q^{(1)\top} C Q^{(1)} = \begin{bmatrix} C_p^{(1)} & C_C^{(1)\top} \\ C_C^{(1)} & C_I^{(1)} \end{bmatrix}.$$

After performing the congruence transformation, original system can be seen as the cascade of a system $\Sigma_1^{(1)}$:

$$\Sigma_1^{(1)} : \begin{cases} G_p^{(1)} x_p^{(1)}(s) + s C_p^{(1)} x_p^{(1)}(s) = B u(s) + u_1^{(1)}(s) \\ y(s) = B^\top x_p^{(1)}(s) \end{cases};$$

and a system $\Sigma_1^{(2)}$:

$$\Sigma_1^{(2)} : \begin{cases} x_I^{(1)}(s) + s C_I^{(1)} x_I^{(1)}(s) = -C_C^{(1)} u_2^{(1)}(s) \\ y^{(2)}(s) = -C_C^\top x_I^{(1)}(s) \end{cases},$$

where $u_1^{(1)}(s) = s y^{(2)}(s)$ and $u_2^{(1)}(s) = s x_p^{(1)}(s)$.

The second step is to perform QR decomposition on the matrix $C_C^{(1)}$ in the system $\Sigma_2^{(1)}$:

$$C_{21}^{(1)} = \tilde{Q}_2 \begin{bmatrix} R^{(2)} \\ 0 \end{bmatrix}.$$

Then we can construct orthogonal transformation $Q^{(1)}$:

$$Q^{(2)} = \begin{bmatrix} I_p & \\ & \tilde{Q}^{(2)} \end{bmatrix}.$$

The coefficient matrix of the original system after orthogonal transformation is

$$\begin{aligned} G^{(2)} \equiv Q^{(2)\top} G^{(1)} Q^{(2)} &= \begin{bmatrix} G_p^{(1)} & & \\ & I_p & \\ & & I_{n-2p} \end{bmatrix}, \\ C^{(2)} \equiv Q^{(2)\top} C^{(1)} Q^{(2)} &= \begin{bmatrix} C_p^{(1)} & R^{(2)\top} & \\ R^{(2)} & C_p^{(2)} & C_C^{(2)\top} \\ C_C^{(2)} & C_I^{(2)} & \end{bmatrix}. \end{aligned}$$

Repeating the process of the second step for another $r-2$ times and retaining only the first rp nodes yields the final reduced-order system: The reduced-order system (5) satisfies the following properties:

- The first $2r$ moments are matched;
- G is block diagonal and C is block tridiagonal;
- The reduced order is rp ;
- All the ports are preserved.

It can be seen that the order of the reduced-order system is proportional to the number of ports; therefore, for multi-port systems, the order reduction efficiency of this method will decrease.

III. MULTIPONT MOMENT MATCHING MODEL ORDER REDUCTION FRAMEWORK

In this section, we introduce the framework of our proposed multipoint moment matching method. We transform the original system into an equivalent structure consisting of a series connection of multiple small systems and one large system via a series of congruence transformations and orthogonal transformations. Then we obtain our reduced-order system by neglecting the large system.

Assume that all of the ports are reordered first and to make the input-output matrices can be represented by

$$B = \begin{bmatrix} B^{(1)} \\ 0 \end{bmatrix}. \quad (6)$$

Then the conductance matrix and the capacitance matrix are represented by

$$G = \begin{bmatrix} G_p & G_C^\top \\ G_C & G_I \end{bmatrix}, C = \begin{bmatrix} C_p & C_C^\top \\ C_C & C_I \end{bmatrix}, \quad (7)$$

where G_p and C_p are p -by- p submatrices of G and C , which represents the connection relationship between ports. The frequency points are

$$S = [s_1, s_2, \dots, s_m], \quad (8)$$

where s_1, s_2, \dots, s_m are nonnegative real numbers.

We first introduce how to perform order reduction for the case of 2 frequency points, then generalize it to the case of multiple points, and present the corresponding moment matching theory.

A. Matching two points

Firstly, we construct a congruence transformation to decouple ports and internal nodes at s_1 . Define matrix A :

$$A \equiv G + s_1 C = \begin{bmatrix} A_p & A_C \\ A_C & A_I \end{bmatrix},$$

which is a positive symmetric matrix. Therefore, A_I is nonsingular. Then original system represented by eq. (1) is equivalent to the following system:

$$\Sigma : \begin{cases} A \begin{bmatrix} x_p(s) \\ x_I(s) \end{bmatrix} + (s - s_1) C \begin{bmatrix} x_p(s) \\ x_I(s) \end{bmatrix} = \begin{bmatrix} B^{(1)} \\ 0 \end{bmatrix} u(s) \\ y(s) = B^{(1)\top} x_p(s) \end{cases}. \quad (9)$$

We can construct the following congruence transformation:

$$W_1 \equiv \begin{bmatrix} I_p & \\ -A_p^{-1} A_C & I_{n-p} \end{bmatrix}.$$

$$\Sigma : \begin{cases} \begin{bmatrix} \widehat{A}_p^{(1)} & \widehat{G}_C^{(1)\top} \\ \widehat{G}_C^{(1)} & \widehat{G}_I^{(1)} \end{bmatrix} \begin{bmatrix} x_p^{(1)}(s) \\ x_I^{(1)}(s) \end{bmatrix} + (s - s_1) \begin{bmatrix} \widehat{C}_p^{(1)} & B_2^\top \\ B_2 & C^{(2)} \end{bmatrix} \begin{bmatrix} x_p^{(1)}(s) \\ x_I^{(1)}(s) \end{bmatrix} = \begin{bmatrix} B^{(1)} \\ 0 \end{bmatrix} u(s) \\ y(s) = B^{(1)\top} x_p^{(1)}(s) \end{cases} \quad (12)$$

Perform the congruence transformation on the matrices G and C , then we can obtain the following matrices:

$$\widehat{G}^{(1)} = W_1^\top G W_1 = \begin{bmatrix} \widehat{G}_p^{(1)} & \widehat{G}_C^{(1)\top} \\ \widehat{G}_C^{(1)} & \widehat{G}_I^{(1)} \end{bmatrix};$$

$$\widehat{C}^{(1)} = W_1^\top C W_1 = \begin{bmatrix} \widehat{C}_p^{(1)} & \widehat{C}_C^{(1)\top} \\ \widehat{C}_C^{(1)} & \widehat{C}_I^{(1)} \end{bmatrix},$$

where

$$\widehat{G}_p^{(1)} = G_p - G_C^\top A_I^{-1} A_C - A_C^\top A_I^{-1} G_C + A_C^\top A_I^{-1} G_I A_I^{-1} A_C;$$

$$\widehat{C}_p^{(1)} = C_p - C_C^\top A_I^{-1} A_C - A_C^\top A_I^{-1} C_C + A_C^\top A_I^{-1} C_I A_I^{-1} A_C;$$

$$\widehat{G}_C^{(1)} = G_C - G_I A_I^{-1} A_C;$$

$$\widehat{C}_C^{(1)} = C_C - C_I A_I^{-1} A_C.$$

They satisfy the following two equations:

$$\widehat{A}_p^{(1)} \equiv \widehat{G}_p^{(1)} + s_1 \widehat{C}_p^{(1)} = A_p - A_C^\top A_I^{-1} A_C; \quad (10)$$

$$\widehat{G}_C^{(1)} + s_1 \widehat{C}_C^{(1)} = 0. \quad (11)$$

Equation (11) implies that the ports and internal nodes are decoupled at s_1 via the congruence transformation W_1 . In elimination-based method such as **SIP**, all internal nodes are neglected. To achieve higher precision, we need to preserve additional internal nodes.

Secondly, we need to construct a orthogonal transformation to determine which internal nodes to preserve. We assume that $\widehat{C}_C^{(1)}$ has the following decomposition:

$$\widehat{C}_C^{(1)} = Q^{(2)} \begin{bmatrix} B^{(2)} \\ 0 \end{bmatrix},$$

where $Q^{(2)}$ is orthogonal matrix and $B^{(2)}$ is an p_2 -by- p matrix and $p_2 \leq p$. The specific decomposition method will be described in detail in section IV. Afterwards, we can define the orthogonal transformation Q_2 :

$$Q_2 \equiv \begin{bmatrix} I_p & \\ & Q^{(2)} \end{bmatrix}.$$

Define matrices

$$G^{(2)} \equiv Q^{(2)\top} \widehat{G}_I^{(1)} Q^{(2)};$$

$$C^{(2)} \equiv Q^{(2)\top} \widehat{C}_I^{(1)} Q^{(2)};$$

$$B_2 \equiv \begin{bmatrix} B^{(2)} \\ 0 \end{bmatrix}.$$

When we perform the transformation W_1 and Q_2 on the system represented by eq. (9), it is equivalent to eq. (12), where $\widehat{A}_p^{(1)}$ is defined as eq. (10). Through equations $u^{(1)}(s) =$

$(s - s_1)y^{(2)}(s)$ and $u_2(s) = (s - s_1)x_p^{(1)}(s)$, system (12) can be seen as the cascade of a system $\Sigma_1^{(1)}$

$$\Sigma_1^{(1)} : \begin{cases} \widehat{G}_p^{(1)} x_p^{(1)}(s) + s \widehat{C}_p^{(1)} x_p^{(1)}(s) = B^{(1)} u(s) + u^{(1)}(s) \\ y(s) = B^{(1)\top} x_p^{(1)}(s) \end{cases} \quad (13)$$

and a system $\Sigma_1^{(2)}$

$$\Sigma_1^{(2)} : \begin{cases} G^{(2)} x_I^{(1)}(s) + s C^{(2)} x_I^{(1)}(s) = -B_2 u_2(s) \\ y_2(s) = -B_2^\top x_I^{(1)}(s) \end{cases}. \quad (14)$$

Block the state vector $x_I^{(1)}$ as

$$x_I^{(1)}(s) = \begin{bmatrix} x_p^{(2)}(s) \\ x_I^{(2)}(s) \end{bmatrix},$$

where the length of $x_p^{(2)}$ is p_2 . Then system $\Sigma_1^{(2)}$ can also be written as

$$\Sigma_1^{(2)} : \begin{cases} G^{(2)} \begin{bmatrix} x_p^{(2)}(s) \\ x_I^{(2)}(s) \end{bmatrix} + s C^{(2)} \begin{bmatrix} x_p^{(2)}(s) \\ x_I^{(2)}(s) \end{bmatrix} = - \begin{bmatrix} B^{(2)} \\ 0 \end{bmatrix} u^{(2)}(s) \\ y_2(s) = -B^{(2)\top} x_p^{(2)}(s) \end{cases}.$$

Although the nodes within $\Sigma_1^{(2)}$ are all internal nodes in the original system represented by eq. (9), they can be divided into ports and internal nodes in $\Sigma_1^{(2)}$. We call the ports in $\Sigma_1^{(2)}$ linear ports because they are connected with the nodes within $\Sigma_1^{(1)}$ but neither input-output ports nor connected with nonlinear elements. All such linear ports need to be preserved.

Thirdly, we decouple the linear ports and the internal nodes in $\Sigma_1^{(2)}$ at expansion point s_2 . Define matrix $A^{(2)}$:

$$A^{(2)} \equiv G^{(2)} + s_2 C^{(2)} = \begin{bmatrix} A_p^{(2)} & A_C^{(2)\top} \\ A_C^{(2)} & A_I^{(2)} \end{bmatrix}.$$

The congruence transformation is written as

$$W_2 = \begin{bmatrix} I_{p_2} & \\ -\left(A_I^{(2)}\right)^{-1} A_C^{(2)} & I_{n-p_1-p_2} \end{bmatrix},$$

and we can obtain

$$\widehat{G}^{(2)} = W_2^\top G^{(2)} W_2 = \begin{bmatrix} \widehat{G}_p^{(2)} & \widehat{G}_C^{(2)\top} \\ \widehat{G}_C^{(2)} & \widehat{G}_I^{(2)} \end{bmatrix};$$

$$\widehat{C}^{(2)} = W_2^\top C^{(2)} W_2 = \begin{bmatrix} \widehat{C}_p^{(2)} & \widehat{C}_C^{(2)\top} \\ \widehat{C}_C^{(2)} & \widehat{C}_I^{(2)} \end{bmatrix}.$$

Perform the congruence transformation on $\Sigma_1^{(2)}$, and the original system can be seen as the cascade of two small systems

$$\Sigma_1^{(1)} : \begin{cases} \widehat{G}_p^{(1)} x_p^{(1)}(s) + s \widehat{C}_p^{(1)} x_p^{(1)}(s) = B^{(1)} u(s) + u^{(1)}(s) \\ y(s) = B^{(1)\top} x_p^{(1)}(s) \end{cases}$$

$$\Sigma_2^{(1)} : \begin{cases} \widehat{G}_p^{(2)} x_p^{(2)}(s) + s \widehat{C}_p^{(2)} x_p^{(2)}(s) = B^{(2)} u_2(s) + u^{(2)}(s) \\ y^{(2)}(s) = B^{(2)\top} x_p^{(2)}(s) \end{cases}$$

and a large system

$$\Sigma_2^{(2)} : \begin{cases} G_I^{(2)} x_I^{(2)}(s) + s C_I^{(2)} x_I^{(2)}(s) = -C_C^{(2)} u_3(s) \\ y^{(3)}(s) = -C_C^{(2)\top} x_I^{(2)}(s) \end{cases},$$

where

$$u_k(s) = (s - s_{k-1}) x_p^{(k-1)}, k = 2, 3;$$

$$u^{(k)}(s) = (s - s_k) y^{(k+1)}(s), k = 1, 2.$$

Finally, the reduced system for the two-point case can be obtained by neglecting $\Sigma_2^{(2)}$, which is represented by eq. (15). From the model order reduction process described above, the two frequency points are not required to be distinct. If the two frequency points satisfy $s_1 = s_2$, a reduced system formulated as eq. (15) can still be obtained; the only difference between these two scenarios lies in the moment matching theory, which will be discussed in the next subsection.

B. Matching more than two points

In this subsection, the number of frequency points m satisfies $m \geq 3$. When we obtain the 2 systems $\Sigma_1^{(1)}$ and $\Sigma_2^{(1)}$ as eqs. (13) and (14), via additional $m - 1$ iterations shown in Appendix A, the original system is transformed into the m small systems

$$\Sigma_1^{(1)} : \begin{cases} \widehat{G}_p^{(1)} x_p^{(1)}(s) + s \widehat{C}_p^{(1)} x_p^{(1)}(s) = B^{(1)} u(s) + u^{(1)}(s) \\ y(s) = B^{(1)\top} x_p^{(1)}(s) \end{cases}; \quad (16)$$

$$\Sigma_2^{(1)} : \begin{cases} \widehat{G}_p^{(2)} x_p^{(2)}(s) + s \widehat{C}_p^{(2)} x_p^{(2)}(s) = -B^{(2)} u_2(s) + u^{(2)}(s) \\ y^{(2)}(s) = -B^{(2)\top} x_p^{(2)}(s) \end{cases}; \quad (17)$$

⋮

$$\Sigma_m^{(1)} : \begin{cases} \widehat{G}_p^{(m)} x_p^{(m)}(s) + s \widehat{C}_p^{(m)} x_p^{(m)}(s) = -B^{(m)} u_m(s) + u^{(m)}(s) \\ y^{(m)}(s) = -B^{(m)\top} x_p^{(m)}(s) \end{cases}; \quad (18)$$

and a large system

$$\Sigma_m^{(2)} : \begin{cases} \widehat{G}_I^{(m)} x_I^{(m)}(s) + s \widehat{C}_I^{(m)} x_I^{(m)}(s) = -C_C^{(m)} u_{m+1}(s) \\ y^{(m+1)}(s) = B^{(m)\top} x_I^{(m)}(s) \end{cases}, \quad (19)$$

where the input vectors and output vectors of the m systems satisfy that

$$u_k(s) = (s - s_{k-1}) x_p^{(k-1)}(s), 2 \leq k \leq m+1;$$

$$u^{(k)}(s) = (s - s_k) y^{(k+1)}(s), 1 \leq k \leq m,$$

and

$$B_m \equiv \begin{bmatrix} -B^{(m)} \\ 0 \end{bmatrix}.$$

Finally, we neglect the large system $\Sigma_m^{(2)}$ and let

$$\tilde{B}^{(k)} = -s_{k-1} B^{(k)}, 2 \leq k \leq m,$$

then the reduced system has been constructed as eq. (20).

C. Moment Matching Analysis

The property of moment matching is given by the following theorem. Consider the multiset $S = \{s_1, s_2, \dots, s_m\}$. We define $q(s_i)$ as the number of appearances of s_i in S .

Theorem 1: The reduced system (20) matches the first $2q(s_i)$ moments of the original system (1) at s_i , $i = 1, 2, \dots, m$.

Proof 1: The proof of the theorem first leverages the moment matching property of the elimination method to derive the moment matching property of the m -th system. Then, by leveraging the recursive relationship between two adjacent systems, the error of the transfer function of the first system is derived. The details are shown in Appendix B.

Theorem 1 shows that when the frequency points satisfy

$$s_1 = s_2 = \dots = s_m,$$

the multipoint moment matching method has the same high-order moment matching properties as **PRIMA** and **TurboMOR**, thus ensuring its precision. However, this method faces the same problem as **TurboMOR**, as illustrated in figs. 1 and 2. Although the system has a block tridiagonal structure, as the number of nodes and ports increases, each diagonal block becomes a dense matrix. This leads to a significant increase in the number of non-zero elements and reducing the efficiency of model order reduction.

IV. ALGORITHM IMPLEMENTATION

This section primarily addresses the densification issue of the reduced-order matrix mentioned at the end of the previous section, and introduces a sparsity control technique and a deflation technique to further improve the multipoint moment matching algorithm.

A. Sparsity Control

The densification of the first diagonal blocks $G_p^{(1)}, C_p^{(1)}$ is caused by the elimination process that retains no internal nodes. To address this issue, we consider eliminating internal nodes one by one in the **AMD** [28] order, and stopping the elimination when the number of non-zero elements reaches a certain threshold. In this paper, this threshold is set to 20 times the dimension of the reduced matrix. This process is illustrated in Algorithm 1. Among the input variables, η is an artificial variable, which means that the elimination process should stop when the non-zero elements of matrix $\widehat{G} + \widehat{C}$ exceeds η times its size. In the following numerical experiment, η takes 20.

$$\begin{cases} \begin{bmatrix} \widehat{G}_p^{(1)} & \tilde{B}^{(2)\top} \\ \tilde{B}^{(2)} & \widehat{G}_p^{(1)} \end{bmatrix} \begin{bmatrix} x_p^{(1)}(s) \\ x_p^{(2)}(s) \end{bmatrix} + s \begin{bmatrix} \widehat{C}_p^{(1)} & B^{(2)\top} \\ B^{(2)} & \widehat{C}_p^{(1)} \end{bmatrix} \begin{bmatrix} x_p^{(1)}(s) \\ x_p^{(2)}(s) \end{bmatrix} = \begin{bmatrix} B^{(1)} \\ 0 \end{bmatrix} u(s) \\ y(s) = B^{(1)\top} x_p^{(1)}(s) \end{cases}. \quad (15)$$

$$\widehat{\Sigma} : \begin{cases} \begin{bmatrix} \widehat{G}_p^{(1)} & \tilde{B}^{(2)\top} & & \\ \tilde{B}^{(2)} & \widehat{G}_p^{(2)} & \ddots & \\ & \ddots & \ddots & \tilde{B}^{(m)\top} \\ & & \ddots & \widehat{G}_p^{(m)} \end{bmatrix} \begin{bmatrix} x_p^{(1)}(s) \\ x_p^{(2)}(s) \\ \vdots \\ x_p^{(m)}(s) \end{bmatrix} + s \begin{bmatrix} \widehat{C}_p^{(1)} & B^{(2)\top} & & \\ B^{(2)} & \widehat{C}_p^{(2)} & \ddots & \\ & \ddots & \ddots & B^{(m)\top} \\ & & \ddots & \widehat{C}_p^{(m)} \end{bmatrix} \begin{bmatrix} x_p^{(1)}(s) \\ x_p^{(2)}(s) \\ \vdots \\ x_p^{(m)}(s) \end{bmatrix} = \begin{bmatrix} B^{(1)} \\ 0 \\ \vdots \\ 0 \end{bmatrix} u(s) \\ y(s) = B^{(1)\top} x_p^{(1)}(s) \end{cases}. \quad (20)$$

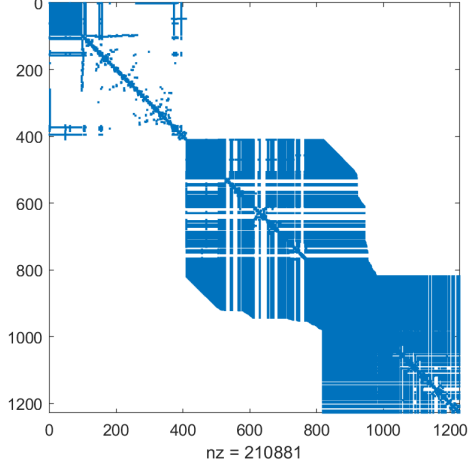


Fig. 1. Nonzero Elements of the Reduced Conductance Matrix in ADC_Net_304

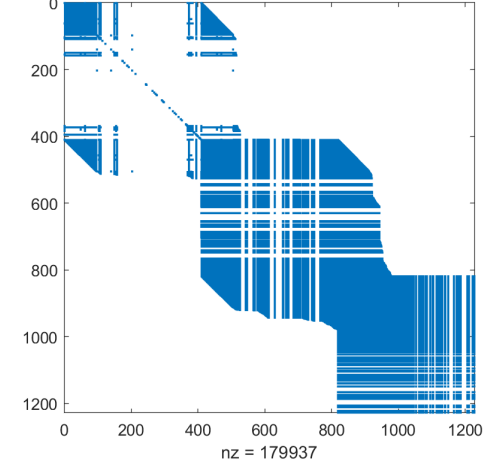


Fig. 2. Nonzero Elements of the Reduced Capacitance Matrix in ADC_Net_304

We assume that the number of the remaining nodes in the first elimination is $p_1 \geq p$. For the elimination of the subsequent subsystem $\Sigma_{k-1}^{(2)}$:

$$\Sigma_{k-1}^{(2)} : \begin{cases} G^{(k)} \begin{bmatrix} x_p^{(k)}(s) \\ x_I^{(k)}(s) \end{bmatrix} + s C^{(k)} \begin{bmatrix} x_p^{(k)}(s) \\ x_I^{(k)}(s) \end{bmatrix} = \begin{bmatrix} -B^{(k)} \\ 0 \end{bmatrix} u^{(k)}(s) \\ y^{(k)}(s) = -B^{(k)\top} x_p^{(k)}(s) \end{cases} \quad (21)$$

where $G^{(k)}$ and $C^{(k)}$ is defined as eqs. (26) and (27), $B^{(k)} \in \mathbb{R}^{p_{k-1} \times p_k}$ and $2 \leq k \leq m$. The coefficient matrices is obtained via orthogonal transformation and is therefore dense. At this point, the more points are eliminated, the fewer nonzero elements remain. For these systems, we directly retain only the linear ports.

B. Deflation

From the previous subsection, we know that the last $m-1$ diagonal blocks of the reduced matrices \widehat{G} and \widehat{C} are dense. Therefore, the fewer linear ports there are in the system represented by eq. (21), the fewer non-zero elements there are in the matrices $G_p^{(k)}$ and $C_p^{(k)}$ in eq. (20). If internal nodes are eliminated without sparsity control, matrix $C_C^{(1)}$ is $n-p$ by p .

However, we find out that in many applications, matrix $C_C^{(1)}$ is nearly rank deficient. To exploit the rank-deficient property of $C_C^{(k)}$, the **RRQR** [29] algorithm can reveal the rank of $C_C^{(k)}$, and the cost is only slightly more than the cost of a regular **QR** factorization. It computes a permutation $P^{(k)}$ and **QR** factorization:

$$C_C^{(k)} P^{(k)} = Q^{(k+1)} \begin{bmatrix} R_{11} & R_{12} \\ & R_{22} \end{bmatrix},$$

where

$$\|R_{22}\|_2 \leq \delta \|R_{11}\|_2.$$

In this article, δ takes 1×10^{-6} , then we have the following decomposition:

$$C_C^{(k)} = Q^{(k+1)} \begin{bmatrix} B^{(k+1)} \\ 0 \end{bmatrix}, k = 1, 2, \dots, m-1,$$

where

$$B^{(k+1)} \equiv [R_{11} \quad R_{12}].$$

Then we have

$$p_m \leq p_{m-1} \leq \dots \leq p_2 < p.$$

Algorithm 1 Sparse SIP

Input G, C, p, s, η .

- 1: All nodes are reordered according to the **AMD** order;
- 2: Place all ports first;
- 3: Compute $\widehat{A} = A = G + sC$;
- 4: $W = I_n$, $\widehat{G} = G$, $\widehat{C} = C$;
- 5: $k = n$;
- 6: while $k > p$
- 7: if $\text{nnz}(\widehat{G} + \widehat{C}) > \eta k$
- 8: break;
- 9: End if
- 10: $\widetilde{A} = \widehat{A}(1 : \text{end} - 1, 1 : \text{end} - 1)$;
- 11: $\widetilde{C} = \widehat{C}(1 : \text{end} - 1, 1 : \text{end} - 1)$;
- 12: $a = \widetilde{A}(1 : \text{end} - 1, \text{end}) / \widetilde{A}(\text{end}, \text{end})$;
- 13: $a_{nn} = \widetilde{A}(\text{end}, \text{end})$;
- 14: $c = \widetilde{C}(1 : \text{end} - 1, \text{end})$;
- 15: $c_{nn} = \widetilde{C}(\text{end}, \text{end})$;
- 16: $\widetilde{A} = \widetilde{A} - a_{nn}aa^\top$;
- 17: $\widetilde{C} = \widetilde{C} - ac^\top - ca^\top + c_{nn}aa^\top$;
- 18: $\widehat{G} = \widehat{A} - s\widetilde{C}$;
- 19: Update W : $W = W \begin{bmatrix} I_{k-1} & & \\ -a^\top & 1 & \\ & & I_{n-k} \end{bmatrix}$;

Output $\widehat{G}, \widehat{C}, W$.

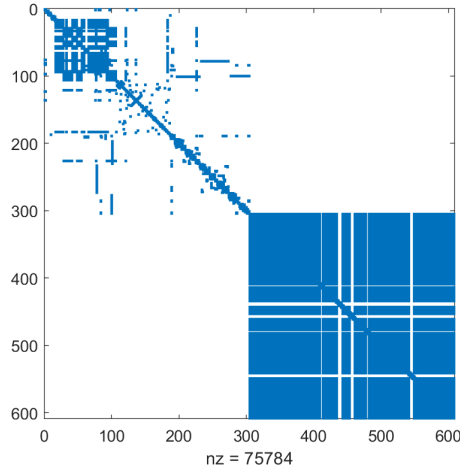


Fig. 3. Nonzero of the Conductance Matrix without Deflation in ADC_Net_27

It means that the order of the reduced system represented by eq. (20) is less than mp . Compared with the system generated by **TurboMOR**, whose order is exactly mp , the impact of an increase in the number of ports on algorithm efficiency will be significantly reduced.

Taking the case ADC_Net_27 as an example, this test case has 304 ports. Here, only 2 frequency points are selected:

$$S = [0; 1 \times 10^6];$$

If the deflation technique is not introduced, the reduced-order matrices obtained through multi-frequency-point elimination is shown in figs. 3 and 4. When we apply deflation, the reduced-order matrices obtained through multi-frequency-point elimination is shown in figs. 5 and 6. By comparing the reduced-order matrices obtained under the two scenarios, we find that the matrix block $\widehat{C}_I^{(2)}$ is dense. After deflation is performed, the size of this block is significantly reduced, which in turn

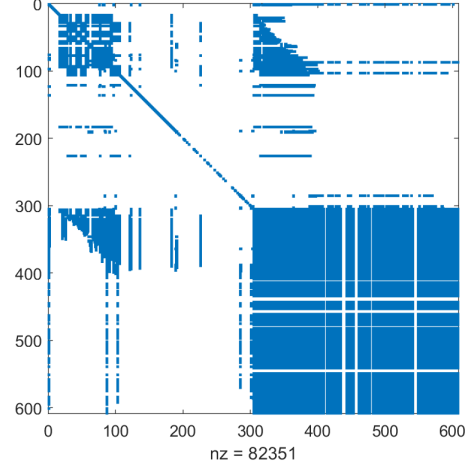


Fig. 4. Nonzero of the Capacitance Matrix without Deflation in ADC_Net_27

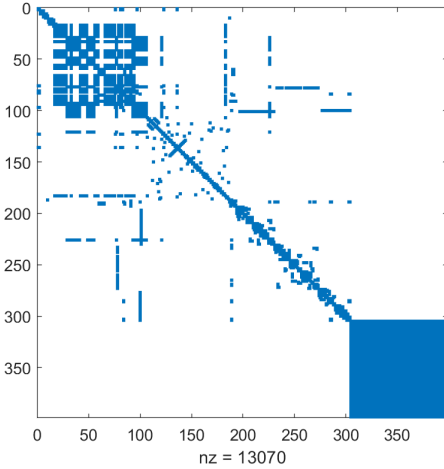


Fig. 5. Nonzero of Conductance Matrix with Deflation in ADC_Net_27

leads to a substantial decrease in the number of non-zero elements of the entire matrix.

C. Implementation

Based on multipoint reduction, we can obtain the frame by combining sparsity control technique and deflation in Algorithm 2.

In the algorithm, the implementation process of the **RRQR** algorithm is detailed in the algorithm of section 3 in the article [29] and that of the **SIP** algorithm is detailed in the algorithm 2 in section 4 in the article [16]. As shown in fig. 7, in the reduced-order system obtained by the optimized algorithm, $G_p^{(1)}$ and $C_p^{(1)}$ are larger sparse matrices, and other diagonal blocks are smaller dense matrix. Compare fig. 7 with fig. 1, the number of nonzero elements decreased by more than 70%.

V. NUMERICAL RESULTS

In this section, we will verify the accuracy of our proposed method and the efficiency of deflation. Afterwards, we will

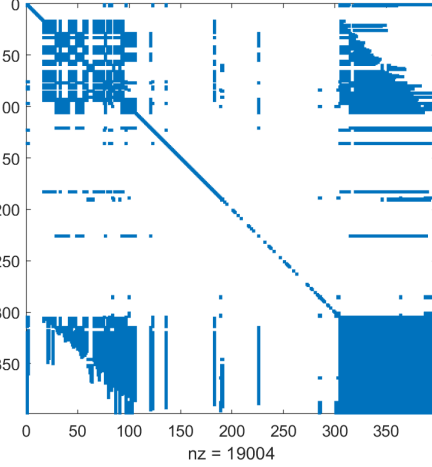


Fig. 6. Nonzero of Capacitance Matrix with Deflation in ADC_Net_27

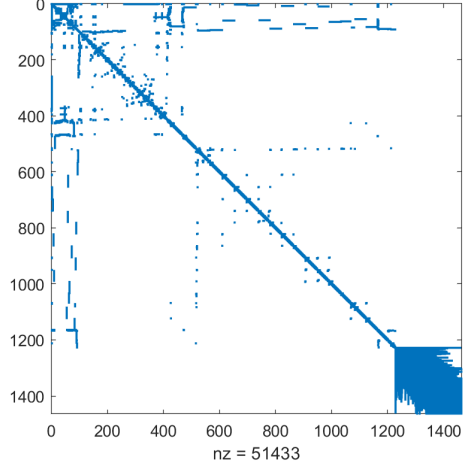


Fig. 7. Nonzero Elements of the Optimized Reduced Conductance Matrix in ADC_Net_304

Algorithm 2 Sparse Multi-Point Matching Method

Input G, C, B, S formulated by eqs. (6) to (8).

- 1: $[\widehat{G}_p^{(1)}, \widehat{C}_p^{(1)}, W_1] = \text{Sparse SIP}(G, C, p, s_1)$;
- 2: Compute $\widehat{G}^{(1)} = W_1^\top G W_1, \widehat{C}^{(1)} = W_1^\top C W_1$
- 3: p_1 is the size of $\widehat{G}_p^{(1)}$;
- 4: **if** $m \geq 2$
- 5: **for** $i = 2 : m$
- 6: Obtain $\widehat{C}_C^{(i-1)}, \widehat{C}_I^{(i-1)}$ and $\widehat{G}_I^{(i-1)}$ formulated in eqs. (24) and (25);
- 7: Apply **RRQR** to compute $C_C^{(i-1)} = Q_i \begin{bmatrix} B^{(i)} \\ 0 \end{bmatrix}$;
- 8: Obtain $G^{(i)}$ and $C^{(i)}$ by eqs. (26) and (27);
- 9: p_i is the columns of $B^{(i)}$;
- 10: $[\widehat{G}_p^{(i)}, \widehat{C}_p^{(i)}, W_i] = \text{SIP}(G^{(i)}, C^{(i)}, p_i, s_i)$;
- 11: Obtain $G^{(i)}$ and $C^{(i)}$;
- 12: $\widehat{G}^{(i)} = W_i^\top G^{(i)} W_i, \widehat{C}^{(i)} = W_i^\top C^{(i)} W_i$;
- 13: **End for**
- 14: Construct \widehat{G} and \widehat{C} as eq. (20);
- 15: $k = \sum_{i=1}^m p_i$;
- 16: $\widehat{B} = B(1 : k, :)$;
- 17: **Else**
- 18: $\widehat{G} = \widehat{G}_p^{(1)}, \widehat{C} = \widehat{C}_p^{(1)}, \widehat{B} = B(1 : p_1, :)$;
- 19: **End if**

Output $\widehat{G}, \widehat{C}, \widehat{B}$.

compare the reduction efficiency with **SIP**, **PRIMA** and **TurboMOR**. Test cases are provided by our industrial partner, as shown in Table I. The #NNZ item is obtained from the explicit system matrix $G+C$. For each resolution circuit, VDD and VSS networks are in the same SPICE file. All experiments are carried out using a single CPU core of a computer cluster running 64-bit CentOS 7.0 with Intel Xeon Gold 6226R @2.90 GHz and 700GB Memory. The wall-clock runtime is reported.

To reduce the fill-ins introduced by **SIP** method, we employ **AMD** [28] ordering for the nodes and control the number of eliminated nodes to ensure the sparsity of the reduced system.

A. Verify Accuracy

In this subsection, we mainly compare the accuracy with **SIP**, and **TurboMOR-RC**. We define the relative errors on

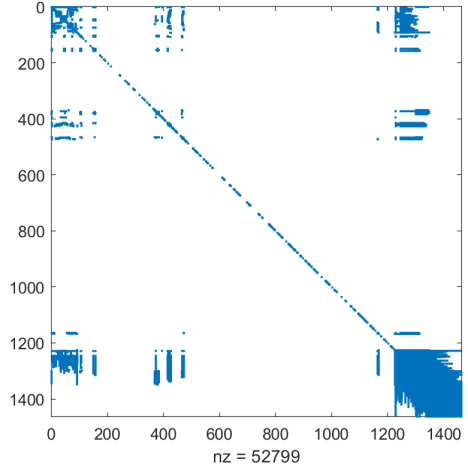


Fig. 8. Nonzero Elements of the Optimized Reduced Capacitance Matrix in ADC_Net_304

frequency f :

$$E_R(f) \equiv \frac{\|H(f) - \widehat{H}(f)\|_2}{\|H(f)\|_2}, \quad (22)$$

$$E_C(f) \equiv \frac{\|H(2\pi\mathcal{J}f) - \widehat{H}(2\pi\mathcal{J}f)\|_2}{\|H(2\pi\mathcal{J}f)\|_2}, \quad (23)$$

TABLE I
INFORMATION OF ORIGINAL SYSTEMS.

Case	Nodes	Ports	nnz($G + C$)
ADC_Net_27	3029	304	19663
ADC_Net_304	4374	409	28808
PLL_Net_1	9500	924	38790
ADC_Net_64	11070	1082	71200
PLL_Net_9	23132	360	106532
PLL_Net_301	1308	59	5848
ADC_Net_1	2044	75	13400

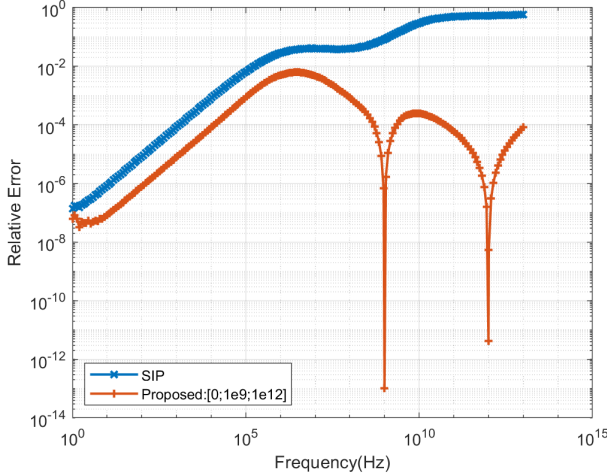


Fig. 9. E_R Comparison with **SIP** at different frequency in PLL_Net_301

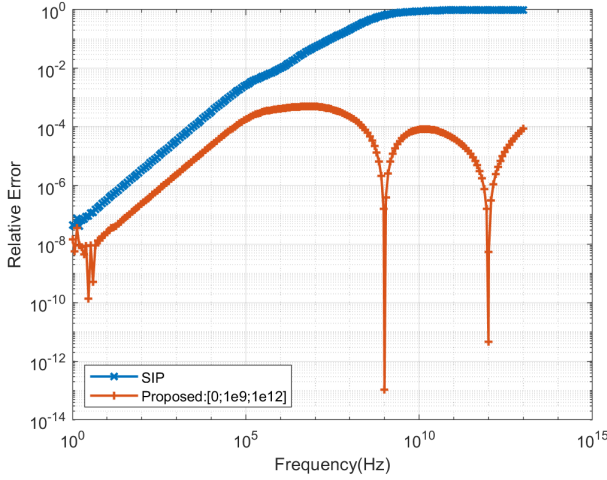


Fig. 10. E_R Comparison with **SIP** at different frequency in ADC_Net_1

where $f \in [0, 10^{13}]$. E_R can verify the multi-point moment matching property of our proposed method. E_C can simulate the relative error of node voltages in simulation to a certain extent.

Firstly, we compare the accuracy of the reduced systems generated by **SIP** and our proposed method. The frequency points are

$$s = [0, 1 \times 10^9, 1 \times 10^{12}].$$

The relative errors E_R at different frequency points are illustrated in figs. 9 and 10. The relative errors E_C at different frequency points are illustrated in figs. 11 and 12. As can be seen from the figures, for the two cases with a few number of ports, **SIP** is insufficient to meet the accuracy requirements in the high-frequency band.

When the order of moment matching in **TurboMOR-RC** takes 8 and the frequency points are

$$s = [0, 0, 1 \times 10^9, 1 \times 10^{12}].$$

The relative error at different frequency points are illustrated in figs. 13 and 14. The relative errors E_C at different frequency

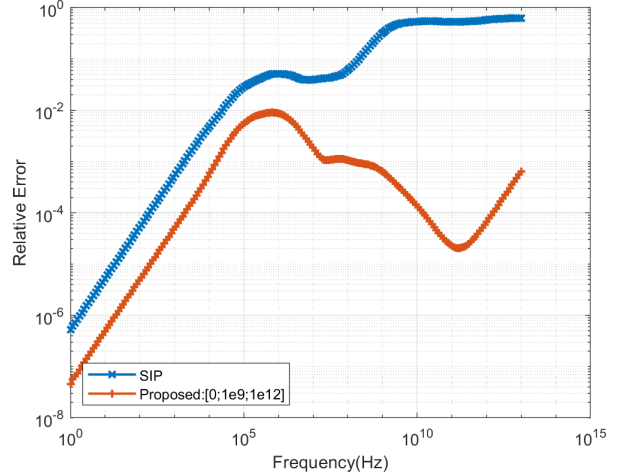


Fig. 11. E_C Comparison with **SIP** at different frequency in PLL_Net_301

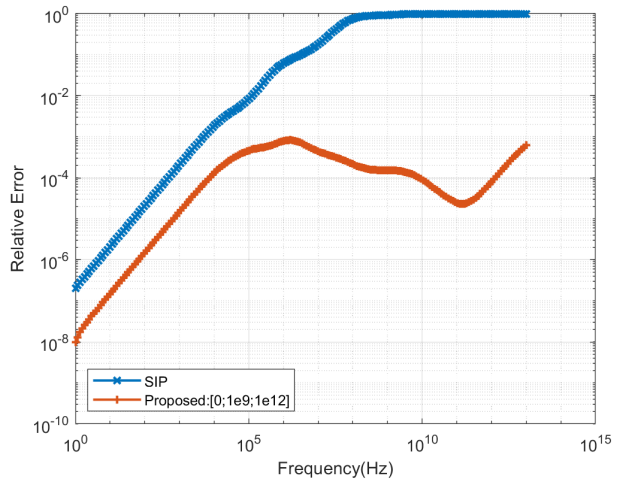


Fig. 12. E_C Comparison with **SIP** at different frequency in ADC_Net_1

points are illustrated in figs. 15 and 16. It can be seen from this that both methods achieve high accuracy in the lower frequency range. However, when the frequency reaches a certain level, our method exhibits higher accuracy compared to **TurboMOR**.

In addition, figs. 9, 10, 13 and 14 reveals that the moment matching properties at 1×10^9 and 1×10^{12} are satisfied.

B. Verify Deflation

To verify the significance of the deflation technique in multi-port cases (the first 5 cases in table I), this subsection compares the number of non-zero elements and accuracy of the reduced-order systems obtained with and without deflation during decomposing matrices $C_C^{(k)}$. The frequency points are

$$s = [0, 1 \times 10^6].$$

The results are shown in table III. The "Reduction Ratio" column indicates the percentage reduction in the number of non-zero elements deflation is applied. As can be seen from

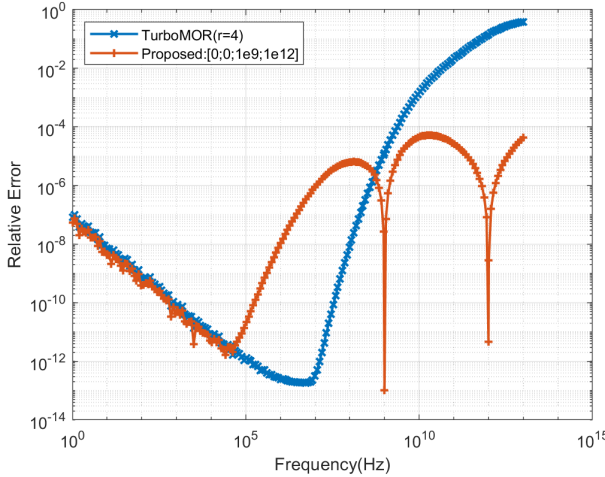


Fig. 13. E_R Comparison with **TurboMOR** at different frequency points in PLL_Net_301($r=4$)

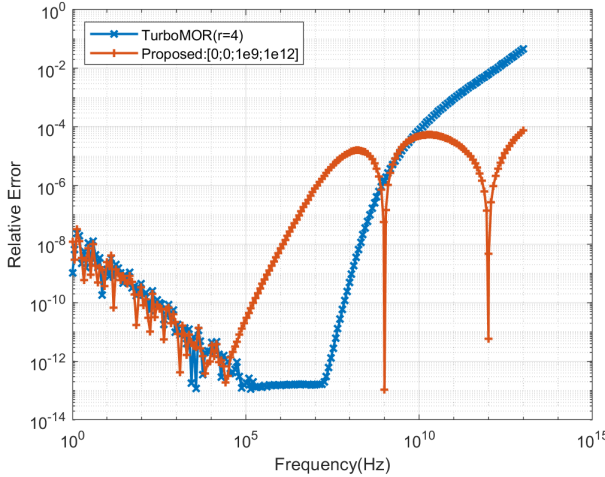


Fig. 14. E_R Comparison with **TurboMOR** at different frequency points in ADC_Net_1($r=4$)

the table, for these test cases, applying deflation significantly reduces the number of non-zero elements in the reduced-order matrix, thereby improving the efficiency of model order reduction. Meanwhile, there is no substantial loss in the accuracy of the reduced-order system.

However, for a specific case (PLL_Net_9), if sparsity control is not implemented, the number of non-zero elements remains unacceptable. In such case we need to apply sparsity control to ensure that our reduced systems are sparse. Then the results of **RC** reduction for PLL_Net_9 are shown in table II. We can observe that when both techniques are used simultaneously, the number of nonzero elements is significantly reduced. In next subsection, we will compare our implemented method with our **RCR** methods.

C. Compare Efficiency

In this subsection, we mainly test the model order reduction efficiency of different algorithms for multi-port RC circuits.

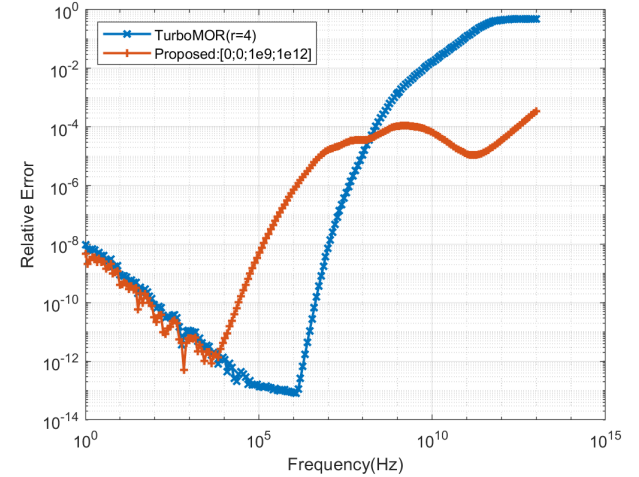


Fig. 15. E_C Comparison with **TurboMOR** at different frequency points in PLL_Net_301($r=4$)

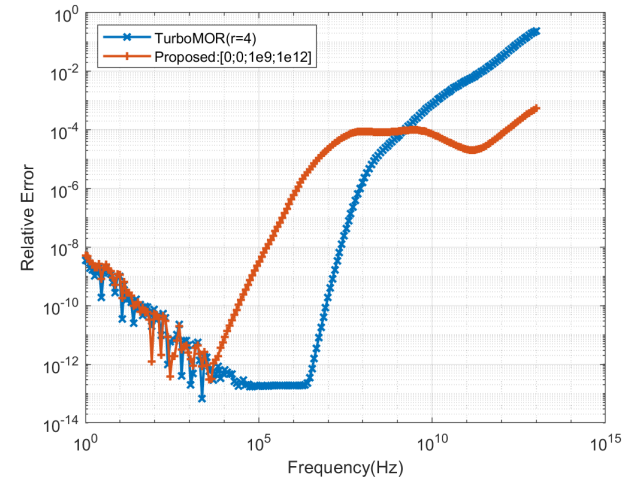


Fig. 16. E_C Comparison with **TurboMOR** at different frequency points in ADC_Net_1($r=4$)

We need to compare both the accuracy at different frequencies and the simulation time of the reduced systems obtained by using the three algorithms. In this case, the simulation time refers to the time required to compute the transfer function. Computing the transfer function involves performing calculations such as matrix multiplications and solving linear equations. When computing $(G + sC)^{-1} B$, We utilize the **KLU** [30] library to perform **LU** factorization and then employ forward substitution and back substitution to solve the p linear systems. The order of moment matching in **PRIMA** and **TurboMOR-RC** takes 4 and the frequency points are

$$s = [0, 1 \times 10^6].$$

The results are revealed in table IV. The simulation time refers to the time taken to compute the transfer functions at 100 frequency points. The "Speed up" column represents the improvement in simulation speed of the reduced-order systems obtained by other algorithms relative to those obtained by the

TABLE II
EFFICIENCY OF IMPLEMENTATION TECHNIQUE IN PLL_NET_9.

Ports	Whether Deflation	Whether Sparsity Control	Nodes	nnz($\widehat{G} + \widehat{C}$)	Reduction Ratio
360	No	No	720	386,292	
	Yes	No	713	381,271	1.30%
	Yes	Yes	12830	135830	64.84%

PRIMA algorithm.

As can be seen from the table, for multi-port **RC** circuits, the reduced-order systems obtained by **TurboMOR** and **PRIMA** contain an excessive number of non-zero elements, which leads to increased simulation time. In contrast, our method not only achieves model order reduction but also maintains an accuracy level comparable to that of these two methods.

Compared with **SIP**, without introducing a significant number of additional linear components (which would undermine the efficiency gains from order reduction), our method can better retain the high-frequency information of the original system, thereby achieving a substantial improvement in accuracy at high-frequency points.

VI. CONCLUSION

To conclude, we propose a multipoint moment matching framework and introduce sparsity control and deflation techniques to guarantee sparsity. Compared to **SIP**, our method significantly improves the accuracy of the reduced-order system at high-frequency points without introducing a large number of additional linear components. Compared to other high-order moment matching methods, our approach significantly reduces the number of non-zero elements in the reduced system, thereby greatly improving simulation speed. This makes our method particularly valuable in applications where high-frequency precision is a key requirement.

APPENDIX A

DETAILS OF THE MULTI-FREQUENCY POINTS REDUCTION PROCESS

In this section, we will present the detailed iterative process of multi-frequency-point reduction, where the number of iterations k is greater than 1. In the k -th iteration, define matrix $A^{(k)}$:

$$A^{(k)} \equiv G^{(k)} + s_k C^{(k)} = \begin{bmatrix} A_p^{(k)} & A_C^{(k)\top} \\ A_C^{(k)} & A_I^{(k)} \end{bmatrix}, k \geq 2.$$

We can construct the congruence transformation W_k to decouple the linear ports and internal nodes in system $\Sigma_{k-1}^{(2)}$:

$$W_k = \begin{bmatrix} I_{p_k} \\ -\left(A_I^{(k)}\right)^{-1} A_C^{(k)} & I \end{bmatrix};$$

$$\widehat{G}^{(k)} = W_k^\top G^{(k)} W_k = \begin{bmatrix} \widehat{G}_p^{(k)} & \widehat{G}_C^{(k)\top} \\ \widehat{G}_C^{(k)} & \widehat{G}_I^{(k)} \end{bmatrix}; \quad (24)$$

$$\widehat{C}^{(k)} = W_k^\top C^{(k)} W_k = \begin{bmatrix} \widehat{C}_p^{(k)} & \widehat{C}_C^{(k)\top} \\ \widehat{C}_C^{(k)} & \widehat{C}_I^{(k)} \end{bmatrix}. \quad (25)$$

Then we decompose matrix $\widehat{C}_C^{(k)}$:

$$\widehat{C}_C^{(k)} = Q^{(k+1)} \begin{bmatrix} B^{(k+1)} \\ 0 \end{bmatrix},$$

where $B^{(k+1)} \in \mathbb{R}^{p_k \times p_{k+1}}$, $p_{k+1} \leq p_k$, and construct orthogonal transformation Q_{k+1} :

$$Q_{k+1} = \begin{bmatrix} I_{p_k} & \\ & Q^{(k+1)} \end{bmatrix}.$$

Then, through orthogonal transformation, we can obtain the conductance matrix and capacitance matrix of the $(k+1)$ -th iteration:

$$G^{(k+1)} \equiv Q^{(k+1)\top} \widehat{G}_{22}^{(k)} Q^{(k+1)}; \quad (26)$$

$$C^{(k+1)} \equiv Q^{(k+1)\top} \widehat{C}_{22}^{(k)} Q^{(k+1)}. \quad (27)$$

After $m-1$ eliminations, the original system can be seen as the cascade of m systems:

$$\Sigma_1^{(1)} : \begin{cases} \left(\widehat{G}_p^{(1)} + s\widehat{C}_p^{(1)}\right)x_p^{(1)} = B^{(1)}u(s) + u^{(1)}(s), \\ y = B^{(1)\top}x_p^{(1)}, \end{cases}$$

$$\Sigma_1^{(2)} : \begin{cases} \left(\widehat{G}_p^{(2)} + s\widehat{C}_p^{(2)}\right)x_p^{(2)} = -B^{(2)}u_2(s) + u^{(2)}(s), \\ y^{(2)} = -B^{(2)\top}x_p^{(2)}, \end{cases}$$

⋮

$$\Sigma_1^{(m-1)} : \begin{cases} \left(\widehat{G}_p^{(m-1)} + s\widehat{C}_p^{(m-1)}\right)x_p^{(m-1)} = -B^{(m-1)}u_{m-1}(s) + u^{(m-1)}(s), \\ y^{(m-1)} = -B^{(m-1)\top}x_p^{(m-1)}, \end{cases}$$

$$\Sigma_{m-1}^{(2)} : \begin{cases} G^{(m)}x_I^{(m-1)}(s) + sC^{(m)}x_I^{(m-1)\top}(s) = -B_m u_m(s), \\ y(s) = -B_m^\top x_I^{(m-1)}(s), \end{cases}$$

where

$$u_k(s) = (s - s_{k-1})x_p^{(k-1)}, 2 \leq k \leq m;$$

$$u^{(k)}(s) = (s - s_k)y^{(k+1)}(s), 2 \leq k \leq m-1.$$

Finally, we decouple the linear ports and the internal nodes in $\Sigma_{m-1}^{(2)}$ at expansion point s_m . Define matrix $A^{(m)}$:

$$A^{(m)} \equiv G^{(m)} + s_m C^{(m)} = \begin{bmatrix} A_p^{(m)} & A_C^{(m)\top} \\ A_C^{(m)} & A_I^{(m)} \end{bmatrix}.$$

The congruence transformation is

$$W_m = \begin{bmatrix} I_{p_m} \\ -\left(A_I^{(m)}\right)^{-1} A_C^{(m)} & I \end{bmatrix},$$

and we can obtain

$$\widehat{G}^{(m)} = W_m^\top G^{(m)} W_m = \begin{bmatrix} \widehat{G}_p^{(m)} & \widehat{G}_C^{(m)\top} \\ \widehat{G}_C^{(m)} & \widehat{G}_I^{(m)} \end{bmatrix};$$

$$\widehat{C}^{(m)} = W_m^\top C^{(m)} W_m = \begin{bmatrix} \widehat{C}_p^{(m)} & \widehat{C}_C^{(m)\top} \\ \widehat{C}_C^{(m)} & \widehat{C}_I^{(m)} \end{bmatrix}.$$

TABLE III
DEFLATION EFFICIENCY OF DIFFERENT CASES.

Case Name	Ports	Whether Deflation	Num. Nodes	nnz($\widehat{G} + \widehat{C}$)	Reduction Ratio	$E_C(1e6)$	$E_C(1e12)$
ADC_Net_27	304	No	608	83,522	76.16%	1.2053e-9	4.3066e-8
		Yes	398	19,914		1.2161e-9	4.4755e-8
ADC_Net_304	409	No	818	102,660	63.90%	1.3710e-10	1.7824e-9
		Yes	526	37,058		1.4308e-10	1.8241e-9
PLL_Net_1	1140	No	1,848	892,946	72.84%	2.7951e-9	1.0615e-8
		Yes	1,140	242,540		2.8844e-9	5.9910e-8
ADC_Net_64	1082	No	2,164	1,035,476	72.87%	5.6848e-9	1.0615e-5
		Yes	1,486	281,900		5.5547e-9	1.1015e-5
PLL_Net_9	360	No	720	386,292	1.30%	3.4303e-8	7.0083e-5
		Yes	713	381,271		3.4303e-8	7.0238e-5

TABLE IV
INFORMATION OF REDUCED SYSTEMS OBTAINED BY DIFFERENT METHODS.

Case Name	Original Time(s)	Method	Num. Nodes	nnz($G + C$)	Simulation Time(s)	Speed up	$E_C(1e9)$	$E_C(1e12)$
ADC_Net_27	0.96	PRIMA	606	369,664	15.04	1 \times	6.3219e-12	1.6467e-8
		TurboMOR	608	31,036	0.84	17.90 \times	6.3099e-12	1.6316e-8
		SIP	304	4,234	0.20	75.20 \times	2.4359e-6	8.6037e-3
		Proposed	398	10,364	0.32	47.00 \times	6.3120e-12	1.3151e-8
ADC_Net_304	1.80	PRIMA	806	649,636	32.28	1 \times	3.2083e-11	1.1742e-9
		TurboMOR	818	129,852	6.51	4.97 \times	3.9964e-11	1.3767e-9
		SIP	2,045	14,019	0.94	50.59 \times	1.9480e-6	2.0618e-3
		Proposed	2,143	27,255	1.28	25.29 \times	2.6984e-11	3.1362e-10
PLL_Net_1	9.22	PRIMA	1,358	1844,164	199.19	1 \times	3.8136e-10	5.6474e-8
		TurboMOR	1,848	309,387	22.51	8.84 \times	3.9934e-10	4.7658e-8
		SIP	3,696	55,584	5.80	34.34 \times	6.4044e-6	1.1701e-3
		Proposed	3,915	94,395	7.08	28.13 \times	3.3859e-10	3.3253e-11
ADC_Net_64	12.15	PRIMA	2,158	4,656,964	710.23	1 \times	2.0020e-11	1.0234e-5
		TurboMOR	2,164	161,931	14.14	50.22 \times	2.0474e-11	1.0234e-5
		SIP	3,246	27,936	4.11	172.80 \times	2.1896e-5	1.3537e-2
		Proposed	3601	48,639	5.73	123.95 \times	2.0005e-11	1.0229e-5
PLL_Net_9	9.95	PRIMA	714	509,796	33.06	1 \times	4.0187e-10	4.2888e-5
		TurboMOR	720	384,770	14.14	50.22 \times	1.0103e-10	4.2888e-5
		SIP	12,600	77,084	5.61	172.80 \times	6.2099e-5	7.7748e-3
		Proposed	12,830	135,830	7.74	123.95 \times	5.4306e-11	3.7866e-5

Perform the congruence transformation on $\Sigma_{m-1}^{(2)}$, and the original system can be seen as the cascade of m small systems

$$\Sigma_1^{(1)} : \begin{cases} \widehat{G}_p^{(1)} x_p^{(1)}(s) + s \widehat{C}_p^{(1)} x_p^{(1)}(s) = B^{(1)} u(s) + u^{(1)}(s) \\ y(s) = B^{(1)\top} x_p^{(1)}(s) \end{cases} ;$$

$$\Sigma_2^{(1)} : \begin{cases} \widehat{G}_p^{(2)} x_p^{(2)}(s) + s \widehat{C}_p^{(2)} x_p^{(2)}(s) = -B^{(2)} u_2(s) + u^{(2)}(s) \\ y^{(2)}(s) = -B^{(2)\top} x_p^{(2)}(s) \end{cases} ;$$

⋮

$$\Sigma_m^{(1)} : \begin{cases} \widehat{G}_p^{(m)} x_p^{(m)}(s) + s \widehat{C}_p^{(m)} x_p^{(m)}(s) = \\ -B^{(m)} u_m(s) + u^{(m)}(s) \\ y^{(m)}(s) = -B^{(m)\top} x_p^{(m)}(s) \end{cases} ;$$

and a large subsystem

$$\Sigma_m^{(2)} : \begin{cases} \widehat{G}_I^{(m)} x_I^{(m)}(s) + s \widehat{C}_I^{(m)} x_I^{(m)}(s) = -C_C^{(m)} u_{m+1}(s) \\ y^{(m+1)}(s) = B^{(m)\top} x_p^{(m)}(s) \end{cases} .$$

APPENDIX B PROOF OF MULTI-FREQUENCY POINTS MATCHING

After $m-1$ eliminations, the original system can be seen as the cascade of m systems represented by eqs. (16) to (19). The transfer function of $\Sigma_2^{(m-1)}$ is denoted by

$$H^{(m)}(s) = B_m^\top \left(G^{(m)} + s C^{(m)} \right)^{-1} B_m.$$

The transfer function of the system obtained by cascading $\Sigma_1^{(1)}, \dots, \Sigma_1^{(m-1)}$ is denoted by $H^{(i)}(s)$, $i = 1, 2, \dots, m-1$.

For system $\Sigma_1^{(m-1)}$, we have

$$\begin{aligned} & \left(\widehat{G}_p^{(m-1)} + s \widehat{C}_p^{(m-1)} \right) x_p^{(m-1)} \\ &= -B^{(m-1)} u_{m-1}(s) + u^{(m-1)}(s) \\ &= -B^{(m-1)} u_{m-1}(s) + (s - s_{m-1}) y^{(m)} \\ &= -B^{(m-1)} u_{m-1}(s) + (s - s_{m-1}) H^{(m)}(s) u_m(s) \\ &= -B^{(m-1)} u_{m-1}(s) + (s - s_{m-1})^2 H^{(m)}(s) x_p^{(m-1)}(s). \end{aligned}$$

Then we can obtain eq. (28). Therefore, we can represent the transfer function of system $\Sigma_1^{(m-1)}$ as eq. (29). Then we have

$$x_p^{(m-1)}(s) = - \left(\widehat{G}_p^{(m-1)} + s\widehat{C}_p^{(m-1)} - (s - s_{m-1})^2 H^{(m)}(s) \right)^{-1} B^{(m-1)} u_{m-1}(s) \quad (28)$$

$$H^{(m-1)}(s) = B^{(m-1)\top} \left(\widehat{G}_p^{(m-1)} + s\widehat{C}_p^{(m-1)} - (s - s_{m-1})^2 H^{(m)}(s) \right)^{-1} B^{(m-1)}. \quad (29)$$

the recurrence relation

$$H^{(i)}(s) = B^{(i)\top} \left(\widehat{G}_p^{(i)} + s\widehat{C}_p^{(i)} - (s - s_i)^2 H^{(i+1)}(s) \right)^{-1} B^{(i)}, \\ i = 1, \dots, m-1.$$

For the reduced model, the m subsystems are represented as eqs. (16) to (18). we have a similar recurrence relation

$$\widehat{H}^{(m)}(s) = B^{(m)\top} \left(\widehat{G}_p^{(m)} + s\widehat{C}_p^{(m)} \right)^{-1} B^{(m)}, \\ \widehat{H}^{(i)}(s) = B^{(i)\top} \left(\widehat{G}_p^{(i)} + s\widehat{C}_p^{(i)} - (s - s_i)^2 \widehat{H}^{(i+1)}(s) \right)^{-1} B^{(i)}, \\ i = 1, \dots, m-1.$$

For any given s_0 , define

$$\delta_i = \begin{cases} 1, & \text{if } s_i = s_0, \\ 0, & \text{otherwise.} \end{cases}$$

Beginning with $\widehat{H}^{(m)}(s) - H^{(m)}(s) = o((s - s_0)^{2\delta_m - 1})$, we can inductively obtain

$$\widehat{H}^{(i)}(s) - H^{(i)}(s) = o((s - s_0)^{2\sum_{j=i}^q \delta_j - 1}), \quad i = 1, \dots, m-1$$

This is because

$$\begin{aligned} & \widehat{H}^{(i)}(s) - H^{(i)}(s) \\ &= B^{(i)\top} \left(\widehat{G}_p^{(i)} + s\widehat{C}_p^{(i)} - (s - s_i)^2 \widehat{H}^{(i+1)}(s) \right)^{-1} B^{(i)} - \\ & \quad B^{(i)\top} \left(\widehat{G}_p^{(i)} + s\widehat{C}_p^{(i)} - (s - s_i)^2 H^{(i+1)}(s) \right)^{-1} B^{(i)} \\ &= (s - s_i)^2 B^{(i)\top} \left(\widehat{G}_p^{(i)} + s\widehat{C}_p^{(i)} - (s - s_i)^2 \widehat{H}^{(i+1)}(s) \right)^{-1} \\ & \quad \left(H^{(i+1)}(s) - \widehat{H}^{(i+1)}(s) \right) \\ & \quad \left(\widehat{G}_p^{(i)} + s\widehat{C}_p^{(i)} - (s - s_i)^2 H^{(i+1)}(s) \right)^{-1} B^{(i)}. \end{aligned}$$

Finally, we have

$$\begin{aligned} \widehat{H}^{(1)}(s) - H^{(1)}(s) &= o((s - s_0)^{2\sum_{j=1}^q \delta_j - 1}) \\ &= o((s - s_0)^{2q(s_0) - 1}), \end{aligned}$$

which completes the proof.

REFERENCES

- [1] Peter Benner, Ulrike Baur, and Lihong Feng. Model order reduction for linear and nonlinear systems: A system-theoretic perspective. *Archives of Computational Methods in Engineering*, 21(4):331–358, December 2014.
- [2] Wilhelmus HA Schilders, Henk A Van der Vorst, and Joost Rommes. *Model order reduction: theory, research aspects and applications*, volume 13. Springer, 2008.
- [3] Jeanne A. Atwell and Belinda B. King. Reduced order controllers for spatially distributed systems via proper orthogonal decomposition. *SIAM Journal on Scientific Computing*, 26(1):128–151, 2004.
- [4] Muruhan Rathinam and Linda R. Petzold. A new look at proper orthogonal decomposition. *SIAM Journal on Numerical Analysis*, 41(5):1893–1925, 2003.
- [5] René Pinnau. *Model Reduction via Proper Orthogonal Decomposition*, pages 95–109. Springer Berlin Heidelberg, Berlin, Heidelberg, 2008.
- [6] C. Mullis and R. Roberts. Synthesis of minimum roundoff noise fixed point digital filters. *IEEE Transactions on Circuits and Systems*, 23(9):551–562, 1976.
- [7] Christian Schröder and Matthias Voigt. Balanced truncation model reduction with a priori error bounds for Lti systems with nonzero initial value. *Journal of Computational and Applied Mathematics*, 420:114708, 2023.
- [8] Roland Pulch and Akil Narayan. Balanced truncation for model order reduction of linear dynamical systems with quadratic outputs. *SIAM Journal on Scientific Computing*, 41(4):A2270–A2295, 2019.
- [9] Nick P. van der Meijs. *Model Order Reduction of Large RC Circuits*, pages 421–446. Springer Berlin Heidelberg, Berlin, Heidelberg, 2008.
- [10] Odabasioglu, Celik, and Pileggi. PRIMA: passive reduced-order interconnect macromodeling algorithm. In *1997 Proceedings of IEEE International Conference on Computer Aided Design (ICCAD)*, pages 58–65, 1997.
- [11] R.W. Freund P. Feldmann. Reduced-order modeling of large linear subcircuits via a block lanczos algorithm. In *32nd Design Automation Conference*, pages 474–479, 1995.
- [12] Nguyen and Jing Li. Multipoint pade approximation using a rational block lanczos algorithm, 1997.
- [13] K. Jbilou and Y. Kaouane. A tangential block lanczos method for model reduction of large-scale first and second order dynamical systems. 81(1):513–536, October 2019.
- [14] H. Barkouki, A. H. Bentbib, and K. Jbilou. An adaptive rational block lanczos-type algorithm for model reduction of large scale dynamical systems. *J. Sci. Comput.*, 67(1):221–236, April 2016.
- [15] Denis Oyaro and Piero Triverio. TurboMOR-RC: An Efficient Model Order Reduction Technique for RC Networks With Many Ports. *IEEE Transactions on Computer-Aided Design of Integrated Circuits and Systems*, 35(10):1695–1706, 2016.
- [16] Zuochang Ye, Dmitry Vasilyev, Zhenhai Zhu, and Joel R. Phillips. Sparse Implicit Projection (SIP) for reduction of general many-terminal networks. In *2008 IEEE/ACM International Conference on Computer-Aided Design*, pages 736–743, 2008.
- [17] Yang Yang, Fan Yang, and Xuan Zeng. Improve sparse implicit projection via incomplete cholesky factorization. In *2023 China Semiconductor Technology International Conference (CSTIC)*, pages 1–3, 2023.
- [18] Roxana Ionutiu, Joost Rommes, and Wil HA Schilders. SparseRC: Sparsity preserving model reduction for RC circuits with many terminals. *IEEE Transactions on Computer-Aided Design of Integrated Circuits and Systems*, 30(12):1828–1841, 2011.
- [19] K.J. Kerns and A.T. Yang. Stable and efficient reduction of large, multiport rc networks by pole analysis via congruence transformations. *IEEE Transactions on Computer-Aided Design of Integrated Circuits and Systems*, 16(7):734–744, 1997.
- [20] B.N. Sheehan. TICER: Realizable reduction of extracted RC circuits. In *1999 IEEE/ACM International Conference on Computer-Aided Design. Digest of Technical Papers (Cat. No.99CH37051)*, pages 200–203, 1999.
- [21] Bernard N. Sheehan. Realizable reduction of rc networks. *IEEE Transactions on Computer-Aided Design of Integrated Circuits and Systems*, 26(8):1393–1407, 2007.
- [22] Limin Hao and Guoyong Shi. High-dimensional extension of the ticer algorithm. *IEEE Transactions on Circuits and Systems I: Regular Papers*, 68(11):4722–4734, 2021.
- [23] Yangfeng Su, Fan Yang, and Xuan Zeng. AMOR: An Efficient Aggregating Based Model Order Reduction Method for Many-Terminal Interconnect Circuits. In *Proceedings of the 49th Annual Design Automation Conference, DAC '12*, pages 295–300, New York, NY, USA, 2012. Association for Computing Machinery.

- [24] Ulrike von Luxburg. A tutorial on spectral clustering. *Statistics and Computing*, 17(4):395–416, December 2007.
- [25] Manar Abdel-Galil, Hazem Hegazy, and Yehea Ismail. RC-In-RC-Out model order reduction via node merging. In *2016 IEEE International Symposium on Circuits and Systems (ISCAS)*, pages 269–272. IEEE, 2016.
- [26] Chung-Wen Ho, Albert Ruehli, and Pierce Brennan. The modified nodal approach to network analysis. *IEEE Transactions on circuits and systems*, 22(6):504–509, 1975.
- [27] Tudor C. Ionescu and Alessandro Astolfi. Moment matching for linear systems – overview and new results*. *IFAC Proceedings Volumes*, 44(1):12739–12744, 2011. 18th IFAC World Congress.
- [28] Patrick R. Amestoy, Timothy A. Davis, and Iain S. Duff. Algorithm 837: AMD, an approximate minimum degree ordering algorithm. *ACM Trans. Math. Softw.*, 30(3):381–388, sep 2004.
- [29] Tony F. Chan. Rank revealing qr factorizations. *Linear Algebra and its Applications*, 88-89:67–82, 1987.
- [30] Timothy A. Davis and Ekanathan Palamadai Natarajan. Algorithm 907: Klu, a direct sparse solver for circuit simulation problems. *ACM Trans. Math. Softw.*, 37(3), September 2010.